Journal of Solid State Chemistry 183 (2010) 3039–3051

Contents lists available at ScienceDirect

Journal of Solid State Chemistry

journal homepage: www.elsevier.com/locate/jssc

Magnetic properties of Fe_2P-type Tb_6FeTe_2, Tb_6CoTe_2, Tb_6NiTe_2 and Er_6FeTe_2 compounds

A.V. Morozkin [a,*], Yu. Mozharivskyj [b], V. SvitlyK [b], R. Nirmala [c], A.K. Nigam [d]

[a] Department of Chemistry, Moscow State University, Leninskie Gory, House 1, Building 3, GSP-2, Moscow 119992, Russia
[b] Department of Chemistry, McMaster University, 1280 Main Street West, Hamilton, Ontario, Canada L8S 4M1
[c] Indian Institute of Technology Madras, Chennai 600 036, India
[d] Tata Institute of Fundamental Research, Mumbai 400 005, India

ARTICLE INFO

Article history:
Received 26 August 2010
Received in revised form
13 October 2010
Accepted 16 October 2010
Available online 30 October 2010

Keywords:
Rare earth intermetallics
Magnetically ordered materials
Magnetocaloric effect
Neutron diffraction

ABSTRACT

The magnetic ordering of the Fe_2P-type Tb_6FeTe_2, Tb_6CoTe_2 Tb_6NiTe_2 and Er_6FeTe_2 phases (space group $P\bar{6}2m$) has been investigated through magnetization measurement and neutron powder diffraction. Tb_6FeTe_2, Tb_6CoTe_2 and Tb_6NiTe_2 demonstrate high-temperature ferromagnetic and low-temperature spin reorientation transitions, whereas Er_6FeTe_2 shows antiferromagnetic transition, only.

The Tb_6FeTe_2 and Tb_6NiTe_2 phases show same high-temperature collinear ferromagnetic structure, whereas Tb_6FeTe_2 is the commensurate non-collinear ferromagnet and Tb_6NiTe_2 is the canted ferromagnetic cone with $\mathbf{K}_1=[0, 0, \pm 3/10]$ and $\mathbf{K}_2=[\pm 2/9, \pm 2/9, 0]$ wave vectors at 2 K. The magnetic structure of Er_6FeTe_2 is a flat spiral with $\mathbf{K}_1=[0, 0, \pm 1/10]$ at 2 K. The magnetic entropy change for Tb_6NiTe_2 is $\Delta S_m=-4.86$ J/kg K at 229 K for the field change $\Delta\mu_0 H=0$–5 T.

In addition, novel Fe_2P-type Gd_6FeTe_2, Zr_6FeTe_2, Hf_6FeTe_2, Dy_6NiTe_2, Zr_6NiTe_2 and Hf_6NiTe_2 phases have been obtained.

1. Introduction

The R_6TX_2 phases (R=Gd–Tm, T=Mn, Fe, Co, Ni, Ru and X=Sb, Bi, Te) are known to adopt a Fe_2P-type structure (space group $P\bar{6}2m$, no. 189) [1–4]. In the Fe_2P-type structure, the R atoms occupy the 3g site (X_{R1}, 0, 1/2) and 3(f) site (X_{R2},0,0), transition metal atoms occupy the special 1b position (0,0,1/2), and antimony (bismuth, tellurium) atoms occupy the special 2c site (1/3,2/3,0) (Fig. 1a). In general, the rare-earth Fe_2P-type compounds demonstrate two ferromagnetic transitions: into a high-temperature collinear ferromagnetic state (Tb_6FeBi_2, Tb_6CoTe_2, Ho_6FeSb_2, Ho_6FeBi_2, Ho_6MnBi_2 and Ho_6CoTe_2) and into a low-temperature non-collinear ferromagnetic state (Tb_6FeBi_2, Ho_6FeSb_2, Ho_6FeBi_2, Ho_6MnBi_2 and Ho_6CoTe_2) [5–7]. Ho_6CoBi_2 shows a high-temperature collinear ferromagnetic ordering, too, but the low-temperature ferromagnetic one has a wave vector $\mathbf{K}=[0, 0, \pm 1/5]$ [7], and Ho_6FeTe_2 has a high-temperature antiferromagnetic ordering and low-temperature ferromagnetic one [8]. No local moment was detected on the transition metal site. Both the nature of the transition metal and the distortion of the unit cell strongly influence the magnetic ordering temperature and the magnetic structure in these compounds. The Mn-containing phases show the highest magnetic ordering temperatures among the whole series.

Magnetocaloric properties have been investigated for Tb_6FeSb_2, Tb_6FeBi_2 [9] and Gd_6CoTe_2 [8]. The Tb_6FeSb_2 has a magnetic entropy change $\Delta S_m=-2.24$ J/kg K at $T_C=256$ K for the field change $\Delta H=0$–2 T, Tb_6FeBi_2 shows $\Delta S_m=-2.56$ J/kg K at $T_C=246$ K for $\Delta H=0$–2 T [8], whereas Gd_6CoTe_2 demonstrates $\Delta S_m=-4.5$ J/kg K at $T_C=220$ K and $\Delta S_m=-6.5$ J/kg K at $T_{CN}=180$ K for $\Delta H=0$–5 T.

To understand the effect of transition metal and p-element atoms on the magnetic properties of novel R_6TX_2 phases has been investigated through the combination of magnetization measurement and neutron powder diffraction.

2. Experimental details

The phases under discussion were prepared by arc-melting in an electric arc furnace under an argon atmosphere using a non-consumable tungsten electrode and a water-cooled copper tray. Pieces of tellurium, zirconium, hafnium (purity 99.99 wt%), gadolinium, terbium, dysprosium, erbium, iron and nickel (99.9 wt% purity for all of the elements) were used as the starting components. Titanium was used as a getter during arc-melting. The arc-melted samples were annealed at 1070 K for 200 h in an argon atmosphere and quenched in ice-cold water.

* Corresponding author.
E-mail address: morozkin@general.chem.msu.ru (A.V. Morozkin).

0022-4596/$ - see front matter © 2010 Elsevier Inc. All rights reserved.
doi:10.1016/j.jssc.2010.10.023

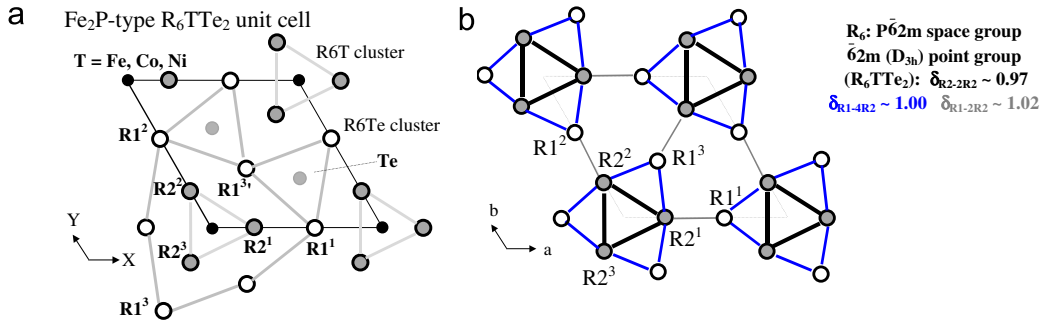

Fig. 1. (a) Unit cell of Fe_2P-type R_6TTe_2 and (b) the $P\bar{6}2m$ s rare-earth sublattice with the *R2*–*2R2*, *R1*–*4R2* and *R1*–*2R2* shortest bonds indicated.

Table 1
Crystallographic data and magnetic properties of the Fe_2P-type R_6FeTe_2 and Tb_6CoTe_2 phases (space group $P\bar{6}2m$, no. 189, atomic sites: *R1* 3(*g*) [X_{R1},0,1/2], *R2* 3(*f*) [X_{R2},0,0], *T* 1(*b*) [0,0,1/2], Te 2(*c*) [1/3,2/3,0]).

Compound	Unit cell data 300 K	Atomic positions at 300 K	R_F (%)	T_{CN} (K) (H=0.05 T)	M_{sat}/R (μ_B)	μ_0H_c (T)	ΔS_m, (J/kg K)	T_{CN}^{ND}, (*K*)	Magnetic structure[c]
Sc_6FeTe_2[a]	a=0.77570 nm c=0.38808 nm								
Y_6FeTe_2[a]	a=0.82065 nm c=0.39984 nm								
Gd_6FeTe_2[b]	a=0.83446(6) nm c=0.40345(2) nm	X_{Gd1}=0.5939(4) X_{Gd2}=0.2417(4)	6.1						
Tb_6FeTe_2[b]	a=0.82753(6) nm c=0.40175(2) nm	X_{Tb1}=0.5945(5) X_{Tb2}=0.2400(5)	5.1	T_C=160 K				T_C^{ND}=160 K	•$\mathbf{F}_C$: $\mathbf{M}^{K0}_{(Tb1,\ Tb2)C}$ (**P31m**), $\mathbf{K}_0$=[0,0,0] (M_{Tb1}=6.2μ_B, M_{Tb2}=9.0μ_B at 50 K)
				T_N=36 K				T_{CN}^{ND}=36 K	•$\mathbf{F}_C-\mathbf{AF}_{ab}-\mathbf{F}_{ab}$: $\mathbf{M}^{K0}_{(Tb1,\ Tb2)C}$ (**P31m**), $\mathbf{M}^{K0}_{(Tb1,Tb2)ab}(\mathbf{Pm_Z})$ (M_{Tb1}=9.0μ_B, M_{Tb2}=9.0μ_B at 2 K)
Tb_6CoTe_2 [6]	a=0.83087(4) nm c=0.39627(2) nm	X_{Tb1}=0.5975(3) X_{Tb2}=0.2382(3)	3.8	T_C=174 K		~2 At 5 K		T_C^{ND}=174 K	•$\mathbf{F}_C$: $\mathbf{M}^{K0}_{(Tb1,\ Tb2)C}$ (**P31m**), $\mathbf{K}_0$=[0,0,0] (M_{Tb1}=5.7μ_B, M_{Tb2}=9.0μ_B at 58 K)
				T_{CN1}=52 K T_{CN2}=27 K				T_{CN}^{ND}=52 K	•$\mathbf{F}_C-\mathbf{AF}_{ab}-\mathbf{F}_{ab}$: $\mathbf{M}^{K0}_{(Tb1,\ Tb2)C}$(**P31m**), $\mathbf{M}^{K0}_{(Tb1,Tb2)ab}(\mathbf{Pm_Z})$ (M_{Tb1}=8.1μ_B, M_{Tb2}=9.0μ_B at 2 K)
Dy_6FeTe_2 [17]	a=0.8236(1) nm c=0.40102(4) nm	X_{Dy1}=0.589(1) X_{Dy2}=0.241(1)	4.3	T_C=135 K T_{CN}=86 K T_m=20 K	8.7 (2 K, 9 T)		−12.5 (9 T) ~0 (9 T)		
Ho_6FeTe_2[b] [8]	a=0.81894(4) nm c=0.39939(2) nm	X_{Ho1}=0.5997(5) X_{Ho2}=0.2386(5)	5.4					T_N^{ND}=24 K	•$\mathbf{AF}_{ab}$: $\mathbf{M}^{K1}_{(Ho1,Ho2)ab}$(flat spiral) $\mathbf{K}_1$=[0,0,±1/9] (M_{Ho1}=6.5μ_B, M_{Ho2}=8.0μ_B at 10 K)
								T_C^{ND}=8 K	•$\mathbf{F}_C-\mathbf{AF}_{ab}$: $\mathbf{M}^{K0}_{(Ho1,Ho2)C}$ (**P31m**) $\mathbf{K}_0$=[0,0,0], $\mathbf{M}^{K1}_{(Ho1,Ho2)ab}$(flat spiral) $\mathbf{K}_1$=[0,0,±1/9] (M_{Ho1}=9.1μ_B, M_{Ho2}=9.6μ_B at 2 K)
Er_6FeTe_2	a=0.81565(8) nm c=0.39827(8) nm	X_{Er1}=0.5967(5) X_{Er2}=0.2407(8)	6.2					T_N^{ND}=18 K	•$\mathbf{AF}_{ab}$: $\mathbf{M}^{K1}_{(Er1,Er2)ab}$ (flat spiral) $\mathbf{K}_1$=[0,0,±1/10] (M_{Er1}=5.6μ_B, M_{Er2}=7.5μ_B at 2 K)
Tm_6FeTe_2[a]	a=0.81038 nm c=0.39715 nm								
Lu_6FeTe_2[a]	a=0.80524 nm c=0.39581 nm								
Zr_6FeTe_2[b]	a=0.77176(3) nm c=0.36346(2) nm	X_{ZR1}=0.5919(5) X_{ZR2}=0.2438(5)	7.2						
Hf_6FeTe_2[b]	a=0.76378(6) nm c=0.35419(4) nm	X_{HF1}=0.5959(5) X_{HF2}=0.2442(5)	7.6						

[a] Tentative from the atomic radii rule.
[b] The crystallographic data used with permission of—© JCPDS—International Centre for Diffraction Data.
[c] **F**—ferromagnetic component; **AF**—antiferromagnetic component. The magnetic component is directed along the *c*-axis ($\mathbf{F}_C$) or lies in the *ab* plane ($\mathbf{F}_{ab}$, $\mathbf{AF}_{ab}$).

The quality of the samples before the neutron diffraction study was evaluated using X-ray diffraction and electron microprobe analysis. The X-ray data were obtained on a diffractometer DRON-3.0 (Cu$K\alpha$ radiation, 2Θ=5–120°, step 0.02°, 10 s/step). The lattice constants were derived using the Rietan-program [10] in the isotropic approximation (Tables 1 and 2).

A "Camebax" microanalyser was employed to perform microprobe X-ray spectral analyses of the samples. The quantitative microprobe analysis of the Fe_2P-type samples gave 66 ± 1,…,2 at% of rare earth, 11 ± 1 at% of iron and 33 ± 1,…, 2 at% of tellurium.

The neutron diffraction studies were carried out on the powder D1B diffractometer [11] (Institute Laue-Langevin, Grenoble, France) from 184 to 2 K for Tb_6FeTe_2, from 28 down to 2 K for Er_6FeTe_2 and from 300 down to 2 K for Tb_6NiTe_2 (temperature step 2–5 K). The neutron diffraction data were refined using the FULLPROF98-program [12].

Table 2
Crystallographic data and magnetic properties of the Fe_2P-type R_6NiTe_2 phases (space group $P\bar{6}2m$, no. 189, atomic sites: $R1$ 3(g) [X_{R1},0,1/2], $R2$ 3(f) [X_{R2},0,0], Ni 1(b) [0,0,1/2], Te 2(c) [1/3,2/3,0]).

Compound	Unit cell data 300 K	Atomic positions at 300 K	R_F (%)	T_{CN} (K) (H=0.01 T)	$\mu_0 H_C$ (T)	ΔS_m[c] (J/kg K)	T_{CN}^{ND} (K)	Magnetic structure[b,d]
Gd_6NiTe_2 [1]	a=0.8412 nm c=0.39577 nm	X_{Gd1}=0.6035 X_{Gd2}=0.2356						
Tb_6NiTe_2[a]	a=0.83464(6) nm c=0.39300(2) nm	X_{Tb1}=0.5932(5) X_{Tb2}=0.2368(5)	6.4	T_C=228 K	~1.5 at 5 K	−4.86	T_C=228 K	$\mathbf{F}_C$: $\mathbf{M}^{K0}_{(Tb1,\ Tb2)C}$ (**P31m**) (M^{K0}_{Tb1}=6.5μ_B, M^{K0}_{Tb2}=6.5μ_B at 100 K)
				T_N=52 K			T_N=55 K	$\mathbf{F}_C-\mathbf{AF}_{ab}$: $\mathbf{M}^{K0}_{(Tb1,\ Tb2)C}$ (**P31m**), $\mathbf{M}^{K1}_{(Tb1,\ Tb2)ab}$ **(flat spiral)** (M^{K0}_{Tb1}=7.0μ_B, M^{K0}_{Tb2}=8.9μ_B, $M^{K1}_{Tb1,2}$=1.24μ_B at 50 K)
				T_{CN}=36 K			T_{CN}=44 K	$\mathbf{F}_C-\mathbf{AF}_{abC}-\mathbf{F}_{ab}$: $\mathbf{M}^{K0}_{(Tb1,\ Tb2)C}$ (**P31m**), $\mathbf{M}^{K0}_{(Tb1,Tb2)ab}$ (**Pm$_z$**), $\mathbf{M}^{K1,K2}_{(Tb1,\ Tb2)ab}$ **(flat spiral)** (M^{K0}_{Tb1}=8.9μ_B, M^{K0}_{Tb2}=8.9μ_B, $M^{K1,K2}_{Tb1,2}$=1.74μ_B at 2 K)
Dy_6NiTe_2[a]	a=0.83021(3) nm c=0.39128(2) nm	X_{Dy1}=0.5946(3) X_{Dy2}=0.2409(3)	4.8					
Zr_6NiTe_2[a]	a=0.76691(3) nm c=0.36953(2) nm	X_{ZR1}=0.5912(4) X_{ZR2}=0.2404(4)	5.0					
Hf_6NiTe_2[a]	a=0.75888(4) nm c=0.35927(2) nm	X_{HF1}=0.5955(5) X_{HF2}=0.2414(4)	6.7					

[a] The crystallographic data used with permission of—© JCPDS—International Centre for Diffraction Data.
[b] **F**—ferromagnetic component; **AF**—antiferromagnetic component. The magnetic component is directed either along the c-axis ($\mathbf{F}_c$), lies in the ab plane ($\mathbf{F}_{ab}$, $\mathbf{AF}_{ab}$) or has some direction in the space ($\mathbf{AF}_{abc}$).
[c] at 229 K, for the 0–5 T field change.
[d] The wave vectors are $\mathbf{K}_0$=[0,0,0], $\mathbf{K}_1$=[0,0,±3/10] and $\mathbf{K}_2$=[±2/9,±2/9,0].

Table 3
Interatomic distances in Tb_6FeTe_2 and Tb_6NiTe_2 and their ratio to the sum of the corresponding atomic radii $\delta=D/(R_{atomic1}+R_{atomic2})$: (a) Tb_6FeTe_2 and (b) Tb_6NiTe_2.

Atom1–Atom2	D (nm)	δ	Coordination number	Atom1–Atom2	D (nm)	δ	Coordination number
Tb1–4Te	0.32177	1.00	13	Tb1–4Te	0.32049	1.00	13
−1Fe	0.33556	1.11		−1Ni	0.33953	1.12	
−4Tb2	0.35462	1.00		−4Tb2	0.35475	1.00	
−2Tb2	0.35554	1.00		−2Tb2	0.35651	1.00	
−2Tb1	0.40175	1.13		−2Tb1	0.39300	1.10	
Tb2–2Fe	0.28248	**0.94**	14	Tb2–2Ni	0.27870	**0.92**	14
−2Te	0.32150	1.00		−2Te	0.32605	1.02	
−2Tb2	0.34400	**0.97**		−2Tb2	0.34233	**0.96**	
−4Tb1	0.35462	1.00		−4Tb1	0.35475	1.00	
−2Tb1	0.35554	1.00		−2Tb1	0.35651	1.00	
−2Tb2	0.40175	1.13		−2Tb2	0.39300	1.13	
Fe–6Tb2	0.28248	**0.94**	11	Ni–6Tb2	0.27870	**0.92**	11
−3Tb1	0.33556	1.11		−3Tb1	0.33953	1.12	
−2Fe	0.40175	1.62		−2Ni	0.39300	1.58	
Te–3Tb2	0.32150	1.00	11	Te–6Tb1	0.32049	1.00	11
−6Tb1	0.32177	1.00		−3Tb2	0.32605	1.02	
−2Te	0.40175	1.40		−2Te	0.39300	1.37	

The dc magnetization was measured on a commercial SQUID magnetometer (Quantum Design) in the 2–300 K temperature range and in the applied field up to 5 T.

3. Results and discussion

3.1. Crystal structure

The structure of the Fe_2P-type R_6TTe_2 phases projected onto the ab plane is shown in Fig. 1a. The Fe_2P-type lattice contains the transition metal and Te sublattices with the $6/mmm$ (D_{6h}) point group and the rare-earth sublattice with the $\bar{6}2m$ (D_{3h}) point group ($P\bar{6}2m$ space group). The rare-earth atoms occupy the following positions: $R1^1$ (X_{R1},0,1/2), $R1^2$ (0,X_{R1},1/2), $R1^3$ ($-X_{R1}$,$-X_{R1}$,1/2); $R2^1$ (X_{R2},0,0), $R2^2$ (0,X_{R2},0) and $R2^3$ ($-X_{R2}$,$-X_{R2}$,0). The shortest $R1$–Te, $R2$–Te, $R1$–$R2$ interatomic distances are close to the sum of metallic radii of pure elements, whereas the $R2$–T and $R2$–$R2$ interatomic distances are less than the sum of metallic radii [13]. The large "transition metal–transition metal" distances preclude the magnetic ordering within the transition metal sublattice. The interatomic distances of Tb_6FeTe_2 and Tb_6NiTe_2 are shown in Table 3. The rare-earth atoms form semi-isolated clusters with the $\bar{6}2m$ (D_{3h}) point group as shown in Fig. 1b.

The a, c cell parameters and the volume of the unit cell, V, of the Fe_2P-type phases increase with the size of R atoms, whereas the c/a ratio shows the opposite trend for the R_6TTe_2 phases (Fig. 2). The dependencies between the lattice parameters and atomic radii for rare-earth compounds are somewhat different from those for the zirconium and hafnium compounds which is most likely due to the different valent states of the rare earths (3+) and zirconium/hafnium (4+), like in Fe_2P-type phases with Sb and Bi [1–3].

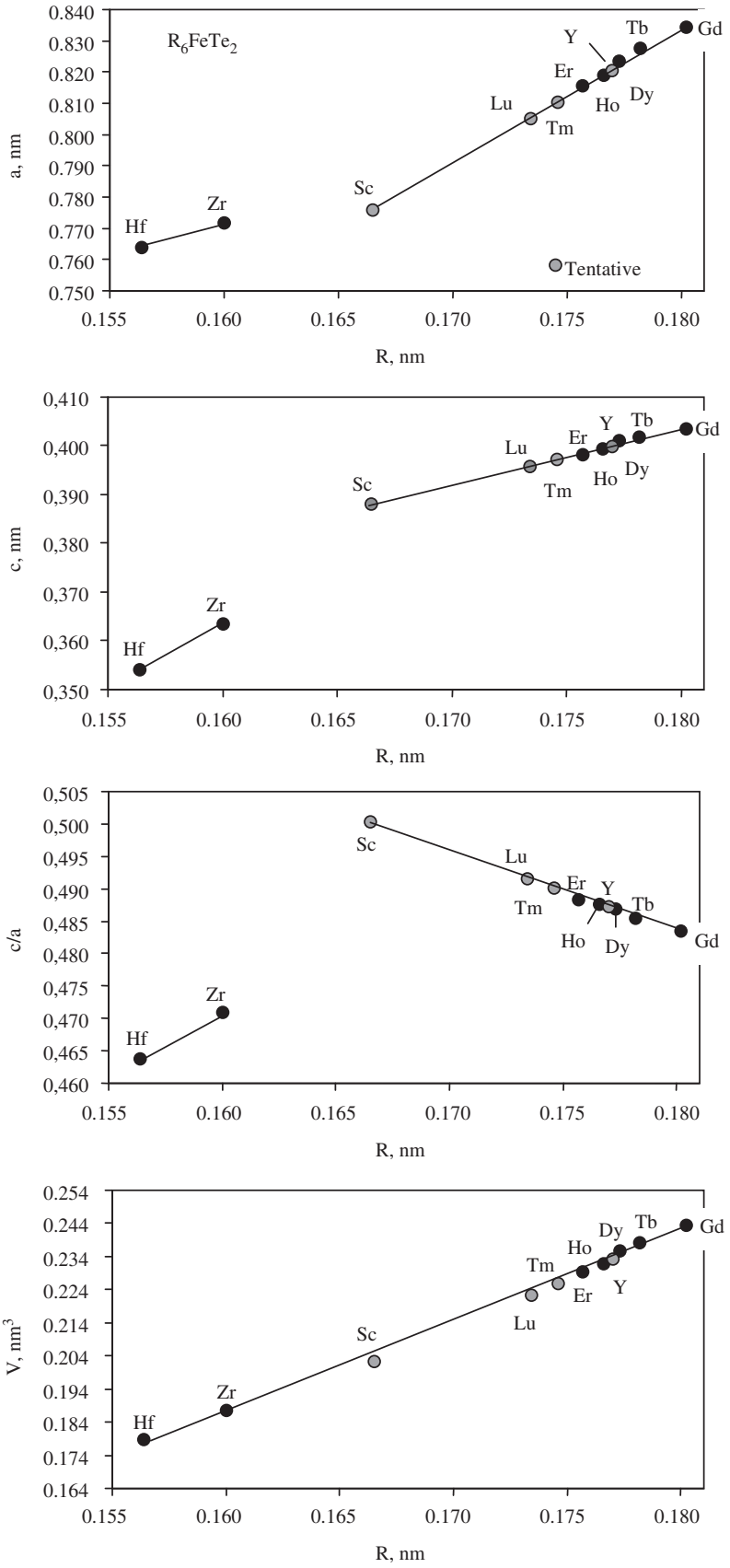

Fig. 2. Cell parameters vs. atomic radii, *R*, of rare earths, zirconium and hafnium for the R_6FeTe_2 phases. The gray symbols correspond to the lattice parameters of hypothetical compounds not studied here but whose lattice parameters are deduced from the general trend of the lanthanide contraction. The error bars are smaller than the corresponding symbols.

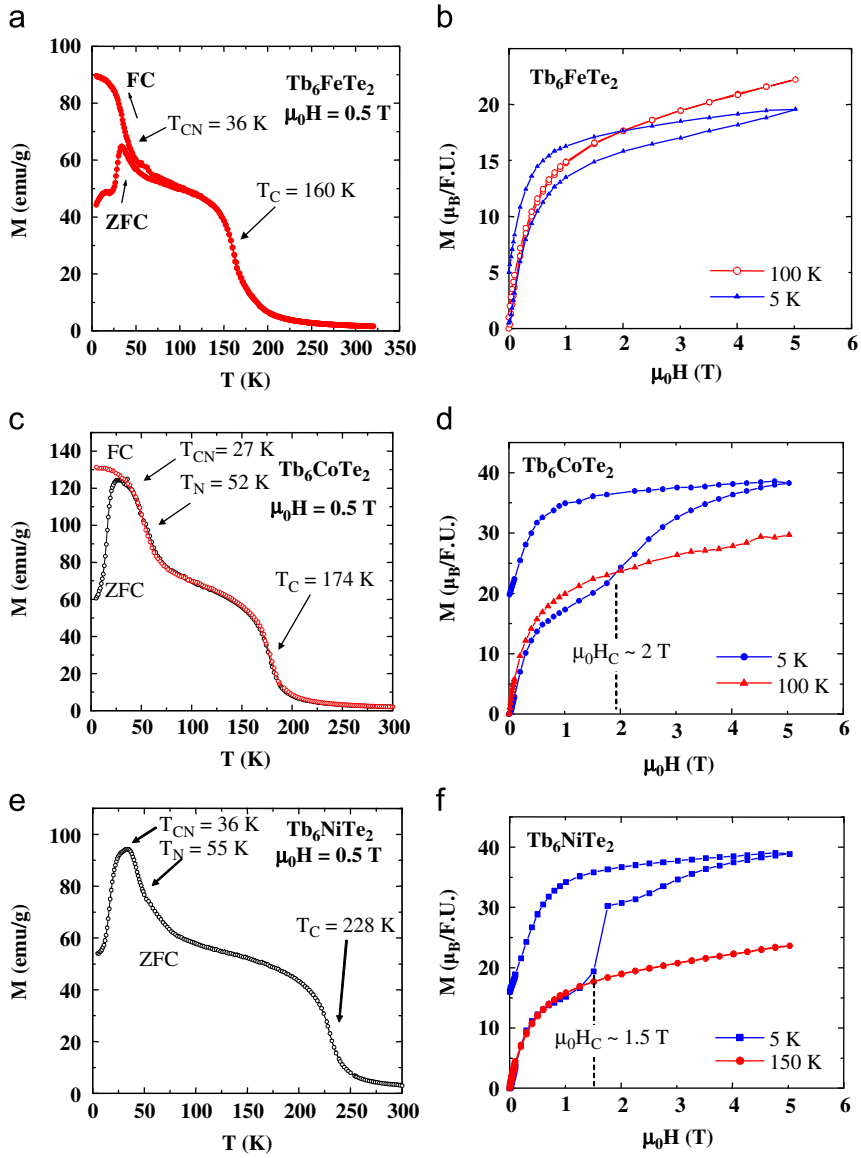

Fig. 3. Magnetization vs. temperature for Tb_6FeTe_2 (a), Tb_6CoTe_2 (c) and Tb_6NiTe_2 (e) and vs. magnetic field for Tb_6FeTe_2 (b), Tb_6CoTe_2 (d) and Tb_6NiTe_2 (f).

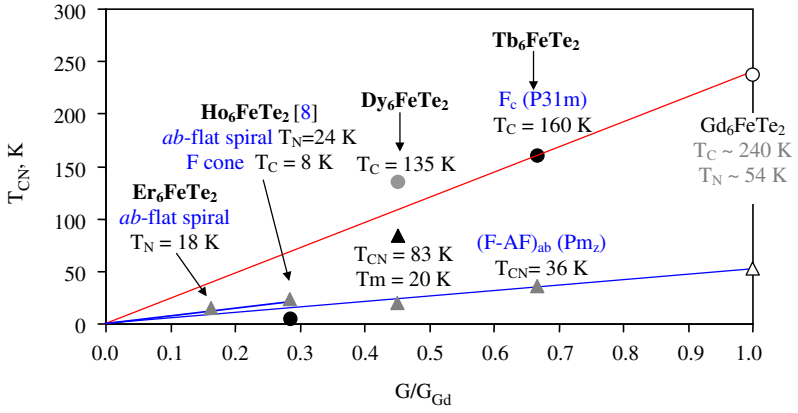

Fig. 4. Magnetic transition temperatures vs. de Gennes factor for R_6FeTe_2 with different magnetic structures (circles represent Curie temperatures, triangles Neel or mixed AF–F transition temperatures). The magnetic transition temperatures for Gd_6FeTe_2 are tentative and derived from de Gennes rule. Details of the $Tb_6FeTe_2$and Er_6FeTe_2 magnetic structures are presented in the ***Magnetic structure*** section.

The Fe_2P-type Sc_6FeTe_2, Y_6FeTe_2, Tm_6FeTe_2 and Lu_6FeTe_2 phases are hypothetical from the chemical properties and crystal structure of Sc, Y, Lu and Tm pure metals [13] and from comparison with seria of Sb- and Bi-containing Fe_2P-type rare earth phases [1–3].

The *a* and *c* parameters for the hypothetical Sc_6FeTe_2, Y_6FeTe_2, Tm_6FeTe_2 and Lu_6FeTe_2 phases with the same structure were extracted from the extrapolation of the corresponding linear fits (Table 1 and Fig. 2). Changes in the lattice parameters of R_6NiTe_2 as a function of the *R* atomic radii is similar to those observed for R_6FeTe_2, and they can be rationalized in terms of the lanthanide contraction.

3.2. Magnetization

Magnetization measurements indicate two or three magnetic transitions for Tb_6FeTe_2, Tb_6CoTe_2 and Tb_6NiTe_2 (Fig. 3 and Tables 1 and 2). The high-temperature magnetic transitions are of a ferromagnetic type, and the low-temperature ones may correspond to the reorientation of magnetic moments and appearance of antiferromagnetic components in the ferromagnetic system. The 5 K magnetization vs. field data reveal metamagnetic transition in the ferromagnetic state for Tb_6CoTe_2 at $\mu_0H_C \sim 2$ T and for Tb_6NiTe_2 at $\mu_0H_C \sim 1.5$ T. The saturation magnetization of Tb_6FeTe_2 at 5 K is lower than that at 100 K, and this is analogous to the Tb_6CoTe_2 behavior below 2 T (Fig. 3). Most likely, the critical field value for Tb_6FeTe_2 is larger than 5 T.

Temperatures of the ferromagnetic transitions in R_6FeTe_2 do not follow the de Gennes rule, while those of the low temperature transitions obey this rule (Fig. 4). Therefore, the high-temperature magnetic structures of Tb_6FeTe_2, Dy_6FeTe_2 and Ho_6FeTe_2 could be different, whereas the low-temperature magnetic structures of Tb_6FeTe_2, Ho_6FeTe_2 and Er_6FeTe_2 could be similar.

3.3. Magnetocaloric effect

The magnetocaloric effect for Tb_6NiTe_2 was evaluated from the magnetization vs. field (*M* vs. *H*) data measured around the Curie temperatures with 7 K increments. The magnetic field changed

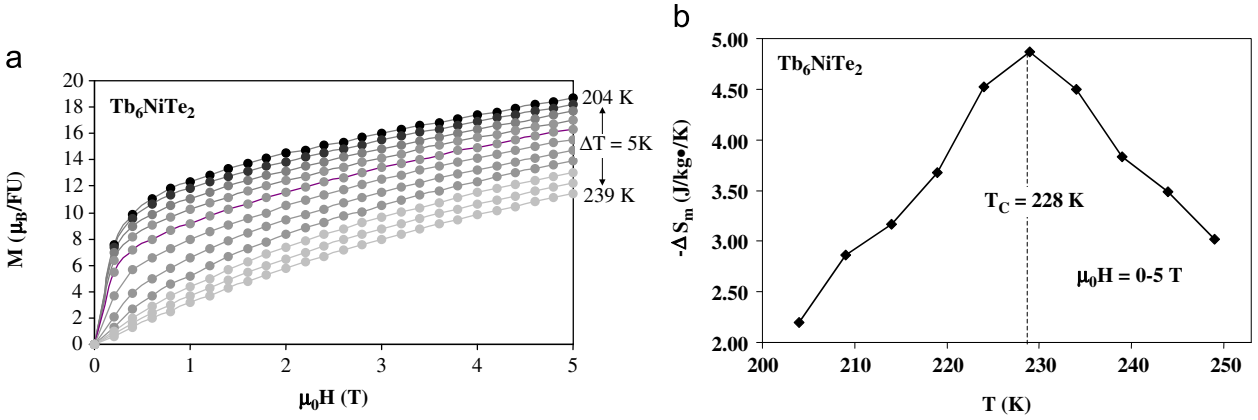

Fig. 5. (a) Magnetization vs. magnetic field and (b) isothermal entropy change, ΔS_m, of Tb_6NiTe_2 as function of temperature.

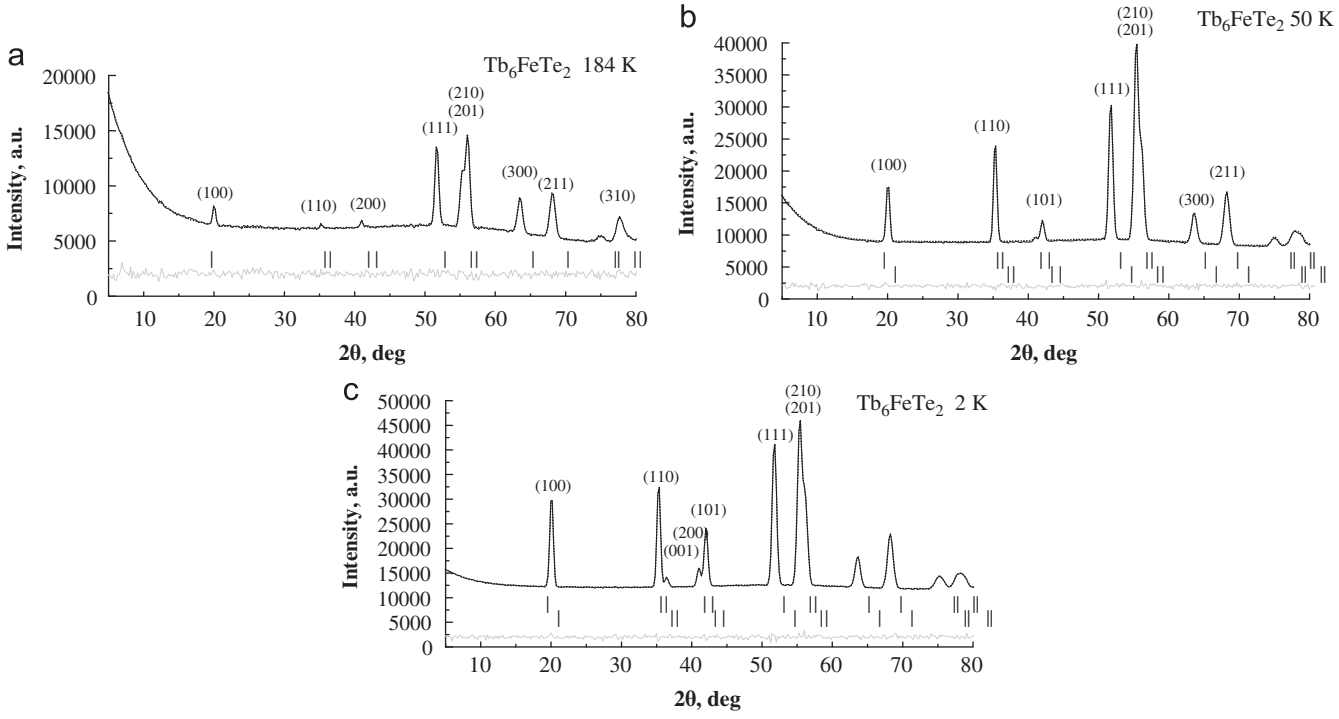

Fig. 6. Neutron diffraction patterns of Tb_6FeTe_2 at (a) 184 K (paramagnetic state), (b) 50 K (collinear ferromagnetic) and (c) 2 K (non-collinear ferromagnetic) ($\lambda = 0.254$ nm).

from 0 to 5 T in 0.2 T steps. MCE in terms of the isothermal entropy change, ΔS_m, was calculated from the magnetization data (Fig. 5a) through the Maxwell equation [14]: $\left(\frac{\partial S(T,H)}{\partial H}\right)_T = \left(\frac{\partial M(T,H)}{\partial T}\right)_H$. Through the integration of the partial derivative of magnetization, M, with respect to temperature, T, over a change in the magnetic field, H, an expression for ΔS is obtained as $\Delta S(T)_{\Delta H} = \int_{H_1}^{H_2} \left(\frac{\partial M(T,H)}{\partial T}\right)_{H,P} dH$. In practice a numerical integration is performed using the following formula: $\Delta S(T)_{\Delta H} = \sum_i \frac{M_{i+1}-M_i}{T_{i+1}-T_i} \Delta H$, where ΔH is a change in magnetic field and M_i and M_{i+1} are the values of magnetization at temperatures T_i and T_{i+1}, respectively.

The magnetocaloric effect for Tb_6NiTe_2 in terms of the isothermal entropy change, $-\Delta S_m$, has the maximum value of 4.86 J/kg K at 229 K for the 0–5 T field change (Fig. 5b). The maximum $|\Delta S_m|$ value is close to the values observed for isostructural Tb_6FeSb_2, Tb_6FeBi_2 [9] and Gd_6CoTe_2 [8] and corresponds to the

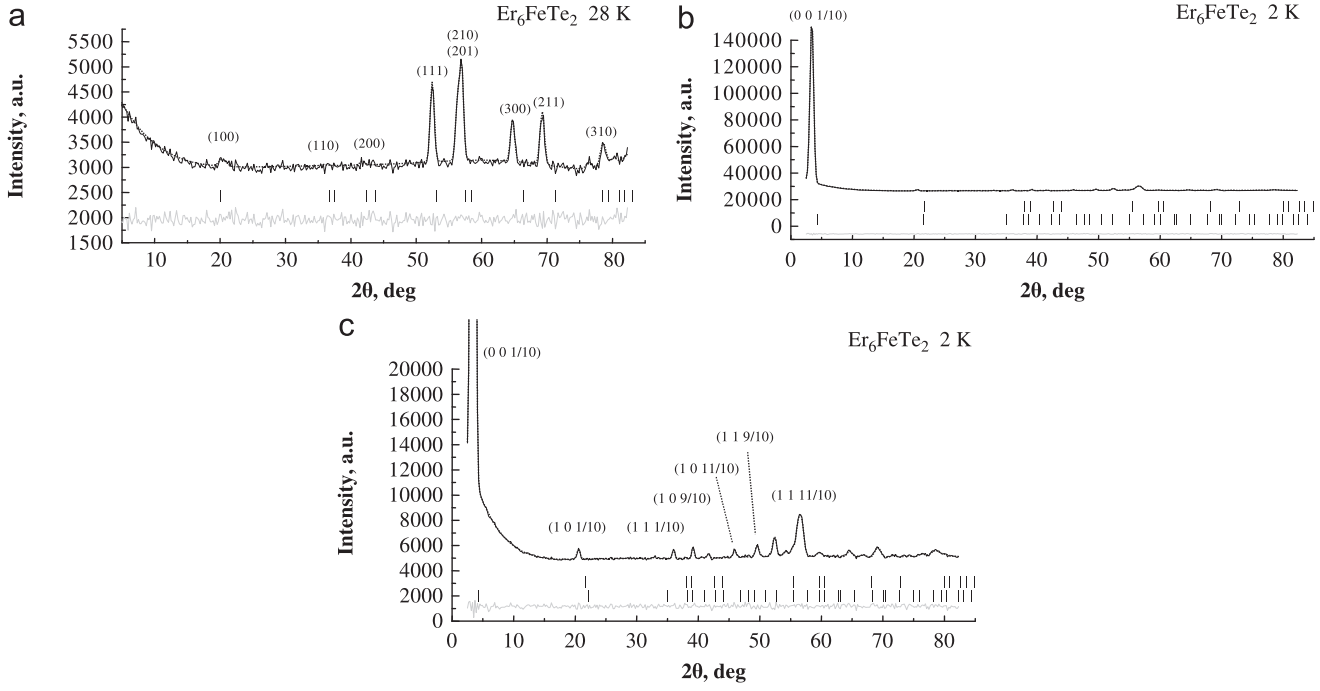

Fig. 7. Neutron diffraction pattern of Er_6FeTe_2 at (a) 28 K (paramagnetic state) and (b, c) 2 K (flat spiral) ($\lambda = 0.254$ nm). Fig. 2b gives the general view of the neutron diffraction pattern at 2 K.

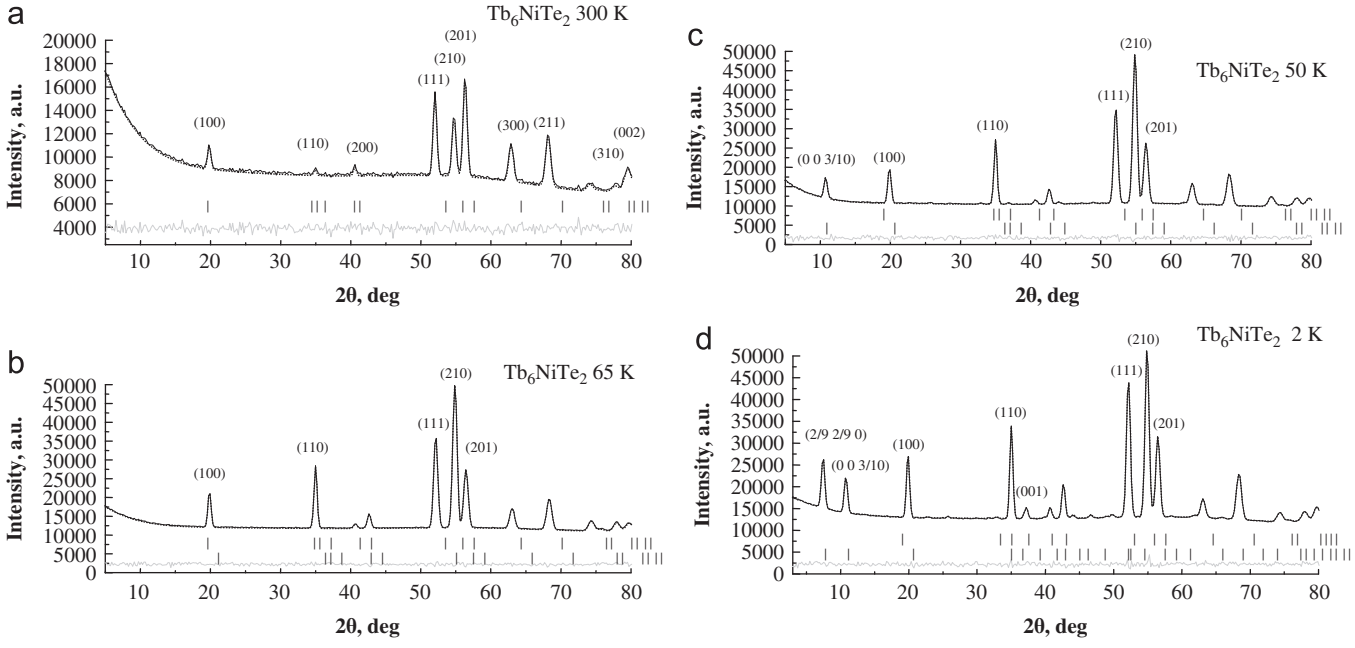

Fig. 8. Neutron diffraction pattern of Tb_6NiTe_2 at (a) 300 K (paramagnetic state), (b) 65 K (collinear ferromagnetic), (c) 50 K (ferromagnetic cone) and (d) 2 K (canted ferromagnetic cone) ($\lambda = 0.254$ nm).

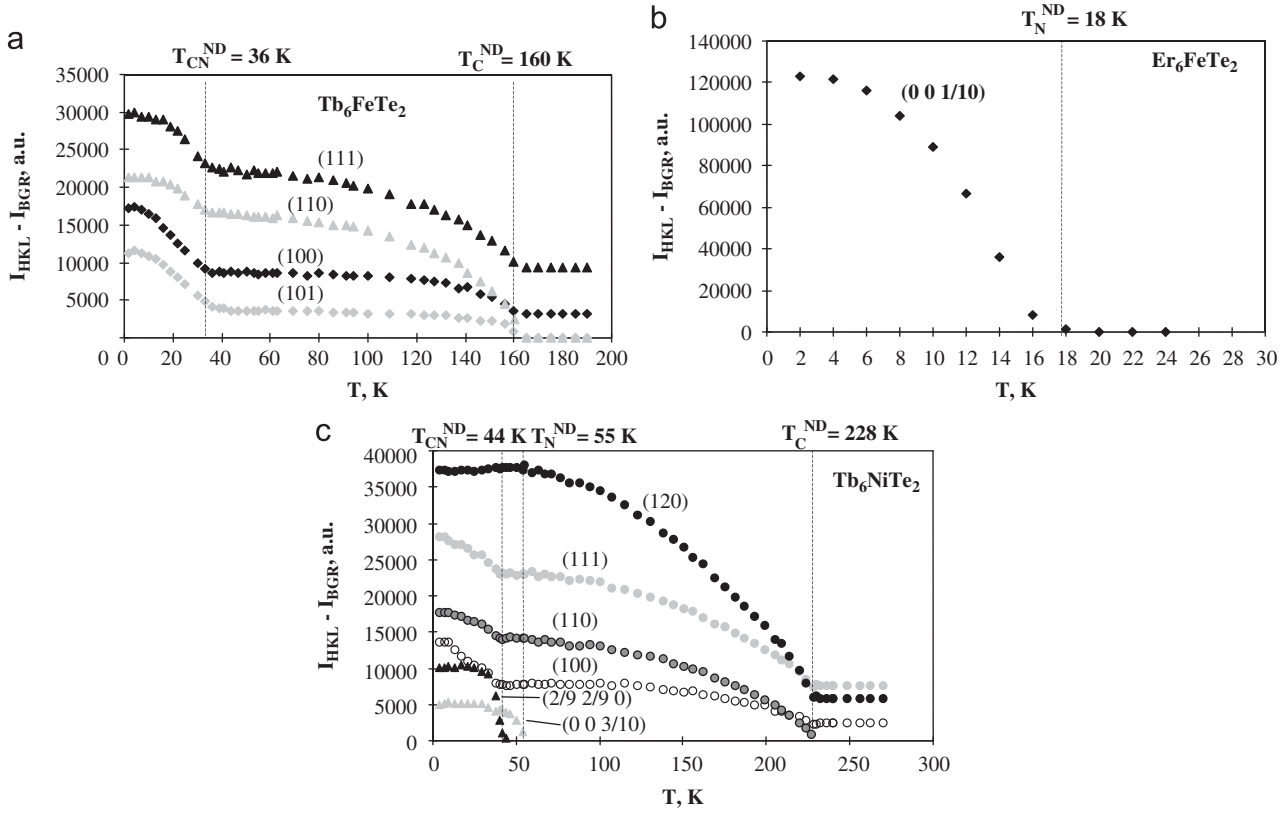

Fig. 9. Thermal variation of intensity of magnetic reflections in (a) Tb_6FeTe_2, (b) Er_6FeTe_2 and (c) Tb_6NiTe_2.

Table 4
Symmetry operations for the general and special sites of the $\bar{6}2m$ (D_{3h}) point group [15].

N	x/a	y/b	z/c	Symmetry operation of general site
1	X	Y	Z	**1**
2	$-Y$	$X-Y$	Z	$\mathbf{3_1}$
3	$-X+Y$	$-X$	Z	$\mathbf{3_2}$
4	X	Y	$-Z$	$\mathbf{m_Z}$
5	$-Y$	$X-Y$	$-Z$	$\mathbf{3_1 m_Z}$
6	$-X+Y$	$-X$	$-Z$	$\mathbf{3_2 m_Z}$
7	Y	X	$-Z$	$\mathbf{2_{XX}}$
8	$X-Y$	$-Y$	$-Z$	$\mathbf{3_1 2_{XX}=2_{XX}3_2=2_X}$
9	$-X$	$-X+Y$	$-Z$	$\mathbf{3_2 2_{XX}=2_{XX}3_1=2_Y}$
10	Y	X	Z	$\mathbf{m_{XX}}$
11	$X-Y$	$-Y$	Z	$\mathbf{3_1 m_{XX}=m_Y}$
12	$-X$	$-X+Y$	Z	$\mathbf{3_2 m_{XX}=m_X}$
N	**x/a**	**y/b**	**z/c**	**Symmetry operation of special site [X_{R1},0,1/2] and [X_{R2},0,0]**
$\mathbf{R1^1}$	X_{R1}	0	1/2	$\mathbf{\{1,m_Z,2_X,m_Y\}}$
$\mathbf{R2^1}$	X_{R2}	0	0	
$\mathbf{R1^2}$	0	X_{R1}	1/2	$\mathbf{\{3_1,3_1 m_Z,2_{XX},m_{XX}\}=\{1,m_Z,2_X,m_Y\}3_1}$
$\mathbf{R2^2}$	0	X_{R2}	0	
$\mathbf{R1^3}$	$-X_{R1}$	$-X_{R1}$	1/2	$\mathbf{\{3_2,3_2 m_Z,2_Y,m_X\}=\{1,\ m_Z\ 2_X,m_Y\}3_2}$
$\mathbf{R2^3}$	$-X_{R2}$	$-X_{R2}$	0	

collinear ferromagnetic ordering of rare-earth magnetic moments along the *c*-axis [5].

3.4. Neutron diffraction study

3.4.1. Magnetic transitions

Figs. 6–8 show the neutron power diffraction patterns recorded at different temperatures in a zero magnetic field for Tb_6FeTe_2, Er_6FeTe_2 and Tb_6NiTe_2. No incommensurate magnetic reflections were detected for Tb_6FeTe_2, both commensurate magnetic reflections with $\mathbf{K}_0=[0,0,0]$ and incommensurate ones with $\mathbf{K}_1=[0,0,\pm 3/10]$ and $\mathbf{K}_2=[\pm 2/9,\pm 2/9,0]$ were observed for Tb_6NiTe_2 and only incommensurate $\mathbf{K}_1=[0,0,\pm 1/10]$ reflections were detected for Er_6FeTe_2. Thermal variations in the intensities of the magnetic reflections indicate magnetic transitions at 160 K and 36 K for Tb_6FeTe_2, at 18 K for Er_6FeTe_2 and at 228, 55 and 44 K for Tb_6NiTe_2 (Fig. 9).

3.4.2. Magnetic structure

The symmetry operations of the $\bar{6}2m$ (D_{3H}) point group are given in Table 4 [15]. This point group includes $D_3=\{C_3, 2_{XX}C_3\}$, $C_{3v}=\{C_3, m_{XX}C_3\}$ and $C_{3H}=\{C_3, m_ZC_3\}$ subgroups of index 2, C_{2v} (D_{1H})$=\{1, m_Z, 2_X, m_Y\}$, $\{1, m_Z, 2_{XX}, m_X\}$, $\{1, m_Z, 2_Y, m_{XX}\}$ subgroups of index 3, $C_3=\{1, 3_1, 3_2\}$ subgroups of index 4 and $C_{1v}=\{1, m_Z\}$, $\{1, m_X\}$, $\{1, m_Y\}$, $\{1, m_{XX}\}$, $D_1=\{1, 2_X\}$, $\{1. 2_{XX}\}$, $\{1, 2_Y\}$ subgroups of index 6 [15]. The possible magnetic point groups for the $\bar{6}2m$ (D_{3H}) point group are the above-mentioned "colorless" and "black–white" (Shubnikov) $\{D_3, m_ZD_31'\}$, $\{C_{3v}, m_ZC_{3v}1'\}$, $\{C_{3h}, 2_{XX}C_{3h}1'\}$, $\{C_{1v}, 2_XC_{1v}1'\}$, $\{D_1, m_ZD_11'\}$ point groups. Magnetic symmetries for special directions of the rare-earth magnetic moments on special sites [X_{R1},0,1/2] and [X_{R2},0,0] are given in Fig. 10.

The magnetic structures of the Fe_2P-type phases were determined in terms of the symmetry of the above-mentioned magnetic point groups. The evolution of the magnetic order during cooling can be clearly identified from the development of magnetic reflections for Tb_6FeTe_2, Er_6FeTe_2 and Tb_6NiTe_2 (Figs. 6–8). Magnetic structures and temperatures of the magnetic transitions were determined form the refinements of neutron powder diffraction data. The crystallographic and magnetic parameters for Tb_6FeTe_2, Tb_6NiTe_2 and Er_6FeTe_2 are shown in Tables 5–7. Refined values of the rare-earth magnetic moments have to be compared to the theoretical values of the Tb and Er ions ($M_{Tb3+}=9\ \mu_B$ and $M_{Er3+}=9\mu_B$) in the trivalent state [16].

3.5. Tb_6FeTe_2

Below 160 K, Tb_6FeTe_2 has a collinear magnetic structure with the **C_{3v} (3 m)** magnetic point group (**P31m** magnetic space group) for the Tb sublattice (the Tb magnetic moments are ferromagnetically ordered along the *c*-axis): $\{\mathbf{M}^{K0}_{(Tb1,\ Tb2)C}\}$ (**P31m**) (Fig. 10 (I) and Fig. 11a). The magnetic moments of Tb1 and Tb2 have

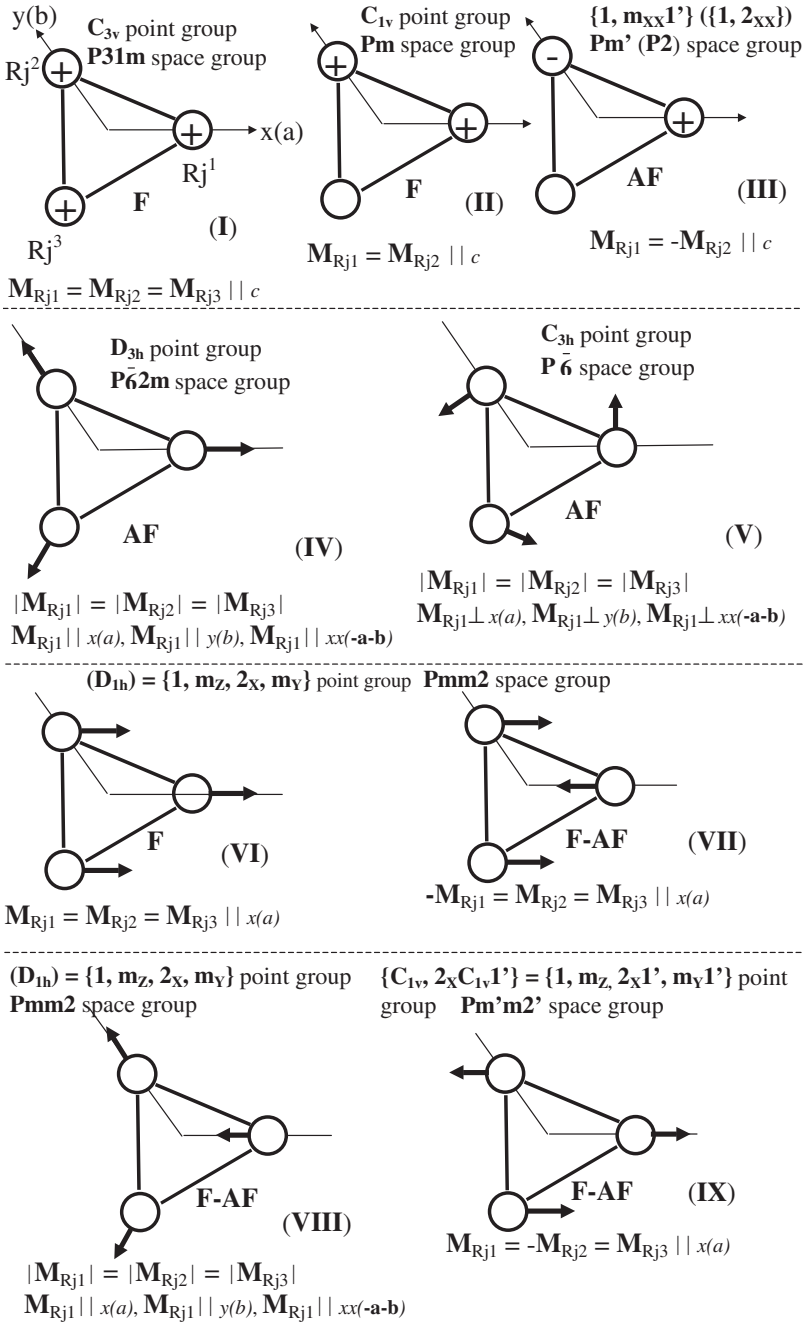

Fig. 10. Magnetic symmetries of the special [X_{R1},0,1/2] and [X_{R2},0,0] sites of the $\bar{6}2m$ (D_{3H}) point group ($P\bar{6}2m$ space group).

Table 5
Crystallographic and magnetic parameters of the Fe_2P-type Tb_6FeTe_2 phase.

T_{CN}	T_{CN}^{ND}	Type	T[a]	Unit cell data	R_F	Atom	M_j^{K0}	φ_j^{K0}	θ_j^{K0}	R_F^m
		Paramagnetic	300[b]	a=0.82753(6) nm c=0.40175(2) nm X_{Tb1}=0.5945(5) X_{Tb2}=0.2400(5)	5.1					
		Paramagnetic	193	a=0.82655(5) nm c=0.40148(3) nm X_{Tb1}=0.5966(7) X_{Tb2}=0.2394(6)	8.5					
160	160	$\mathbf{F}_C$:$\mathbf{M}^{K0}_{(Tb1,\ Tb2)C}$ (**P31m**)	50	a=0.82534(5) nm c=0.40084(3) nm X_{Tb1}=0.5975(6) X_{Tb2}=0.2400(4)	5.6	$Tb1^1$ $Tb1^2$ $Tb1^3$ $Tb2^1$ $Tb2^2$ $Tb2^3$	6.2(1) 6.2(1) 6.2(1) 9.0(1) 9.0(1) 9.0(1)	0 0 0 0 0 0	0 0 0 0 0 0	5.2
36	36	$\mathbf{F}_C-\mathbf{AF}_{ab}-\mathbf{F}_{ab}$:$\mathbf{M}^{K0}_{(Tb1,Tb2)ab}$ ($\mathbf{Pm_Z}$) $\mathbf{M}^{K0}_{(Tb1,\ Tb2)C}$ (**P31m**)	2	a=0.82519(5) nm c=0.40069(3) nm X_{Tb1}=0.5976(7) X_{Tb2}=0.2395(3)	3.6	$Tb1^1$ $Tb1^2$ $Tb1^3$ $Tb2^1$ $Tb2^2$ $Tb2^3$	9.0(2) 9.0(2) 9.0(2) 9.0(2) 9.0(2) 9.0(2)	−42(2) 42(2) 42(2) 42(2) −42(2) −42(2)	52(1) 52(1) 52(1) 15(1) 15(1) 15(1)	5.6

T_{CN} (K) and T_{CN}^{ND} (K) are the magnetic transition temperatures from magnetic measurements and neutron diffraction studies. **F** a ferromagnetic component, **AF** an antiferromagnetic component. X_{Tb1} and X_{Tb2} are the atomic position parameters. M_j^{K0} (μ_B) is the magnetic moment of the corresponding atom with wave vectors $\mathbf{K}_0$=[0,0,0]; φ_j^{K0} and θ_j^{K0} are the angles (deg) of the corresponding magnetic moment with the a and c axes. Reliability factors R_F (crystal structure) and R_F^m (magnetic structure) are given in percent (%).

[a] Temperature for which the crystallographic and magnetic parameters are reported for a given magnetic state.
[b] X-ray data.

Table 6
Crystallographic and magnetic parameters of the Fe_2P-type Tb_6NiTe_2 phase.

T_{CN}	T_{CN}^{ND}	Type of magnetic ordering	T[a]	Unit cell data	R_F	Atom	M_j^{K0}	φ_j^{K0}	θ_j^{K0}	$M_j^{K1,\ K2}$	Wave vector	R_F^m
		Paramagnetic	300[b]	a=0.83464(6) nm c=0.39300(2) nm X_{Tb1}=0.5932(5) X_{Tb2}=0.2368(5)	6.4							
		Paramagnetic	300	a=0.8343(2) nm c=0.3933(1) nm X_{Tb1}=0.597(1) X_{Tb2}=0.234(1)	5.2							
	228	$\mathbf{F}_C$: $\mathbf{M}^{K0}_{(Tb1,\ Tb2)C}$ (**P31m**)	100	a=0.8326(1) nm c=0.39261(7) nm X_{Tb1}=0.596(1) X_{Tb2}=0.236(1)	2.7	$Tb1^1$ $Tb1^2$ $Tb1^3$ $Tb2^1$ $Tb2^2$ $Tb2^3$	6.5(2) 6.5(2) 6.5(2) 8.7(2) 8.7(2) 8.7(2)	0 0 0 0 0 0	0 0 0 0 0 0			2.4
52	55	$\mathbf{F}_C-\mathbf{AF}_{ab}$: $\mathbf{M}^{K0}_{(Tb1,\ Tb2)C}$ (**P31m**) $\mathbf{M}^{K1}_{(Tb1,\ Tb2)ab}$ **(flat spiral)**	50	a=0.8326(1) nm c=0.39250(6) nm X_{Tb1}=0.596(1) X_{Tb2}=0.235(1)	3.6	$Tb1^1$ $Tb1^2$ $Tb1^3$ $Tb2^1$ $Tb2^2$ $Tb2^3$	7.0(2) 7.0(2) 7.0(2) 8.9(2) 8.9(2) 8.9(2)	0 0 0 0 0 0	0 0 0 0 0 0	1.24(3) 1.24(3) 1.24(3) 1.24(3) 1.24(3) 1.24(3)	$\mathbf{K}_1$	5.2
33	44	$\mathbf{F}_C-\mathbf{AF}_{abC}$-$\mathbf{F}_{ab}$:$\mathbf{M}^{K0}_{(Tb1,Tb2)ab}$ ($\mathbf{Pm_Z}$) •$\mathbf{M}^{K0}_{(Tb1,\ Tb2)C}$ (**P31m**) •$\mathbf{M}^{K1,\ K2}_{(Tb1,\ Tb2)ab}$ **(flat spiral)**	2	a=0.83272(9) nm c=0.39259(6) nm X_{Tb1}=0.597(1) X_{Tb2}=0.235(1)	2.6	$Tb1^1$ $Tb1^2$ $Tb1^3$ $Tb2^1$ $Tb2^2$ $Tb2^3$	8.9(2) 8.9(2) 8.9(2) 8.9(2) 8.9(2) 8.9(2)	−36(2) 36(2) 36(2) 36(2) −36(2) −36(2)	45(2) 45(1) 45(2) 11(2) 11(2) 11(1)	1.74(3) 1.74(3) 1.74(3) 1.74(3) 1.74(3) 1.74(3)	$\mathbf{K}_1$, $\mathbf{K}_2$	3.8

T_{CN} (K) and T_{CN}^{ND} (K) are the magnetic transition temperatures from magnetic measurements and neutron diffraction studies. **F** a ferromagnetic component, **AF** an antiferromagnetic component. X_{Tb1} and X_{Tb2}, are the atomic position parameters. M_j^{K0}, $M_j^{K1,\ K2}$ (μ_B) are the magnetic moments of the corresponding atom with wave vectors $\mathbf{K}_0$=[0,0,0], $\mathbf{K}_1$=[0,0, ± 3/10] and $\mathbf{K}_2$=[± 2/9, ± 2/9,0]. φ_j^{K0} and θ_j^{K0} are the angle (deg) of corresponding magnetic moments with the a and c axes. The cone axis of the flat spirals with $\mathbf{K}_1$ and $\mathbf{K}_2$ coincides with the magnetic moment directions of the corresponding atom, the cone angles $\beta_j^{K1}=\beta_j^{K2}$=90 deg. Reliability factors R_F (crystal structure) and R_F^m (magnetic structure) are given in percent (%).

[a] Temperature for which the crystallographic and magnetic parameters are reported for a given magnetic state.
[b] X-ray data.

significantly different values (Table 5). Below 36 K, the reflections indicate ferromagnetic and anteferromagnetic orderings in the *ab* plane (Fig. 6c). The (VII), (VIII) and (IX) variants of the magnetic symmetry (Fig. 10) would agree with such behavior. Variant (VII) has a good agreement with experimental data ($\mathbf{D_{1H}}$=**{1**, $\mathbf{m_Z}$, $\mathbf{2_X}$, $\mathbf{m_Y}$**}** point group, **Pmm2** space group) (Fig. 11b), but the best fit is achieved for a "canted" ferromagnetic ordering with the $\mathbf{C_{1v}}$=**{1**, $\mathbf{m_Z}$**}** magnetic point group ($\mathbf{Pm_Z}$ magnetic space group) shown in

Table 7
Crystallographic and magnetic parameters of the Fe_2P-type Er_6FeTe_2 phase.

T_C^{ND}	Type	T[a]	Unit cell data	R_F	Atom	M_j	R_F^m
	Paramagnetic	300[b]	a=0.81565(8) nm c=0.39827(8) nm X_{Er1}=0.5967(5) X_{Er2}=0.2407(8)	6.2			
	Paramagnetic	28	a=0.8154(6) nm c=0.3977(5) nm X_{Er1}=0.599(4) X_{Er2}=0.239(4)	7.8			
18	**AF$_{ab}$:** $\{M_{Er1}, M_{Er2}\}^{K1}$ **(flat spiral)**	2	a=0.8147(4) nm c=0.3975(4) nm X_{Er1}=0.596(4) X_{Er2}=0.236(4)	6.7	Er1^1 Er1^2 Er1^3 Er2^1 Er2^2 Er2^3	5.6(2) 5.6(2) 5.6(2) 7.5(2) 7.5(2) 7.5(2)	3.0

T_N^{ND} (K) is the magnetic transition temperature from the neutron diffraction studies. **AF** an antiferromagnetic component. X_{Er1} and X_{Er2}, are the atomic position parameters. M_j (μ_B) is the magnetic moment of the corresponding atom with wave vectors $\mathbf{K_1}$=[0,0,±1/10] (magnetic phase is zero for all atoms, cone angle is 90°, cone axis coincides with the c-axis). Reliability factors R_F (crystal structure) and R_F^m (magnetic structure) are given in percent (%).

[a] Temperature for which the crystallographic and magnetic parameters are reported for a given magnetic state.
[b] X-ray data.

Fig. 11c. Thus, below 36 K the Tb_6FeTe_2 magnetic structure becomes a non-collinear ferromagnet due to the presence of magnetic point group $\mathbf{C_{1v}}$=**{1, m$_z$}** with the ab components: $\{\mathbf{M}^{K0}_{(Tb1,\ Tb2)abC}\}$ (**P1**)=$\{\mathbf{M}^{K0}_{(Tb1,\ Tb2)C}\}$ (**P31m**)+$\{\mathbf{M}^{K0}_{(Tb1,\ Tb2)ab}\}$ (**Pm$_z$**). Models with other magnetic point groups had no satisfactory agreement with the experimental data. The magnetic structure projected onto the ab plane consists of collinear, ferromagnetically ordered domains (Fig. 11c).

The symmetry of the high-temperature magnetic ordering (**P31m**) closes the symmetry of the rare-earth sublattice ($P\bar{6}2m$ space group), whereas the low-temperature magnetic ordering leads to a decrease in the magnetic symmetry down to **P1**.

The thermal variations of the terbium magnetic moments are shown in Fig. 12a. Details of the Tb_6FeTe_2 magnetic structure are given in Table 5.

3.6. Tb_6NiTe_2

Below 228 K, Tb_6NiTe_2 has a collinear magnetic structure with the $\mathbf{C_{3v}}$ (**3 m**) magnetic point group (**P31m** magnetic space group) for the Tb sublattice (the Tb magnetic moments are ferromagnetically ordered along the c-axis) (Fig. 10 (I) and Fig. 11a): $\{\mathbf{M}^{K0}_{(Tb1,\ Tb2)C}\}$ (**P31m**), like in Tb_6FeTe_2 and Tb_6CoTe_2 [6]. The magnetic moments of Tb1 and Tb2 have strongly different values (Table 6).

Below 55 K the magnetic structure of Tb_6NiTe_2 is a ferromagnetic cone. The terbium magnetic components with a $\mathbf{K}_0$=[0,0,0] wave vector are ferromagnetically coupled and directed along the c-axis ($\{\mathbf{M}^{K0}_{(Tb1,\ Tb2)C}\}$ (**P31m**)), whereas the terbium magnetic component with a $\mathbf{K}_1$=[0,0,±3/10] wave vector (flat spiral: cone angle 90°, magnetic phase is zero for all atoms) are arranged in the ab plane (Fig. 11d).

Below 44 K the commensurate part of Tb_6NiTe_2 magnetic structure becomes a non-collinear ferromagnet due to the presence of magnetic point group $\mathbf{C_{1v}}$=**{1, m$_z$}** for the ab components: $\{\mathbf{M}^{K0}_{(Tb1,\ Tb2)abC}\}$ (**P1**)=$\{\mathbf{M}^{K0}_{(Tb1,\ Tb2)C}\}$ (**P31m**)+$\{\mathbf{M}^{K0}_{(Tb1,\ Tb2)ab}\}$ (**Pm$_z$**), like in Tb_6FeTe_2 and Tb_6CoTe_2 [6] (Fig. 11c), whereas the incommensurate part of the Tb_6NiTe_2 magnetic structure is a set of flat spirals with the $\mathbf{K}_1$=[0,0,±3/10] and $\mathbf{K}_2$=[±2/9,±2/9,0] wave vectors (cone angle 90°, magnetic phase is zero for all atoms, cone axes coincide with the directions of the commensurate magnetic moments of the corresponding atoms). The magnetic structure consists of canted ferromagnetic cones (Fig. 11e). The thermal variations of the terbium magnetic moments are shown in Fig. 12b. Details of the Tb_6NiTe_2 magnetic structure are given in Table 6.

The following decrease in symmetry is observed for the terbium sublattice: $P\bar{6}2m$ (paramagnetic state) →**P31m** (high-temperature magnetic ordering) →**P1** (low-temperature magnetic ordering).

3.7. Er_6FeTe_2

Below 18 K Er_6FeTe_2 is a pure antiferromagnet and its magnetic structure is a flat spiral with wave vector $\mathbf{K}_1$=[0,0,±1/10] (the cone axis coincides with the c-axis, cone angle is 90°, magnetic phase is zero for all atoms) (Fig. 11d). The magnetic structure consists of ferromagnetically ordered (in the ab plane) Er magnetic moments that rotate along the c-axis, and it is similar to the high-temperature magnetic structure of Ho_6FeTe_2 [8]. The thermal variations of the erbium magnetic moments are shown in Fig. 12c. The magnetic moments of Er1 and Er2 have different values. Details of the Er_6FeTe_2 magnetic structure are given in Table 7. The symmetry of the erbium sublattice decreases from $P\bar{6}2m$ (paramagnetic state) to **P1** (antiferromagnetic ordering).

The Tb_6FeTe_2, Tb_6CoTe_2 [6] and Tb_6NiTe_2 have the same high-temperature and commensurate low-temperature magnetic structures. In general, the magnetic moments of the $R2$ site are bigger than those of the $R1$ site: $M_{R2} > M_{R1}$. Due to specific features of the low-temperature magnetic structure the Ho_6FeTe_2 and Tb_6FeTe_2 compounds show metamagnetic transition in mixed magnetic state, similar to the Tb_6CoTe_2 and Tb_6NiTe_2 systems (Figs. 3 and 11).

The symmetry of the rare-earth sublattice in pure rare-earth metals ($P6_3/mmc$, $\mathbf{D_{6H}}$ point group) is close to that in Fe_2P-type phases ($P\bar{6}2m$, $\mathbf{D_{3H}}$ point group). For this reason, the magnetic structure of the corresponding Fe_2P-type phases correlates with the magnetic structure of the corresponding pure rare earths: Tb_6FeTe_2, Tb_6CoTe_2 and Tb_6NiTe_2 have the magnetic structures similar to those of pure Tb [16], Ho_6FeTe_2 [6] and Er_6FeTe_2 have the magnetic structures similar to those of Ho and Er [16].

The structural and magnetic role of the transition metals (Fe, Co, Ni) in the Fe_2P-type phases is not quite clear. Their atomic radii are unlikely to determine the distortion of the rare-earth sublattices as the $R2$–T distances are smaller than the sum of metallic radii (Table 3), however the cell parameters do correlate with the size of the transition metals: $a_{R6NiTe2} > a_{R6CoTe2} > a_{R6FeTe2}$ and $c_{R6NiTe2} < c_{R6CoTe2} < c_{R6FeTe2}$ (Tables 1 and 2). Also the high-temperature magnetic orderings reveal dependence on the

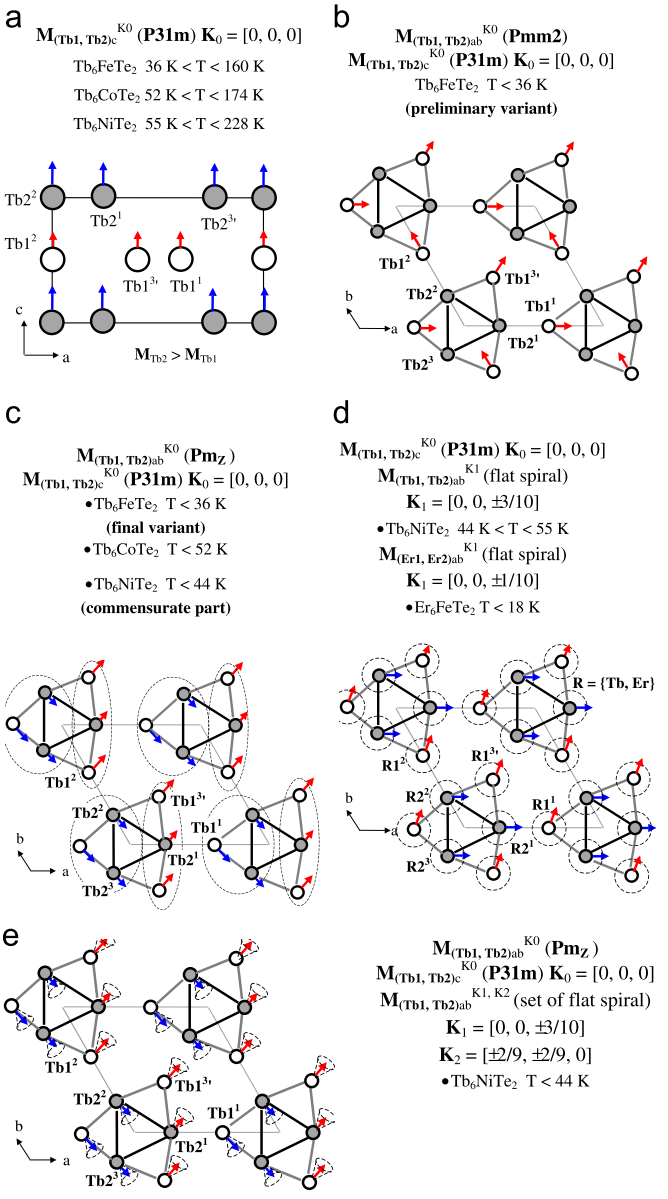

Fig. 11. (a) Magnetic structure of Tb_6FeTe_2, Tb_6CoTe_2 and Tb_6NiTe_2 below the high-temperature ferromagnetic transitions, (b) a preliminary variant of Tb_6FeTe_2, (c) the final variants of Tb_6FeTe_2, Tb_6CoTe_2 and commensurate part of Tb_6FeTe_2 below the low-temperature AF–F transition, (d) the final variants of Tb_6NiTe_2 between T_{CN}=44 K and T_N=55 K of Er_6FeTe_2 below T_N=18 K and (e) of Tb_6NiTe_2 below T_{CN}=44 K (the cone axes coincide with the directions of the commensurate magnetic moments).

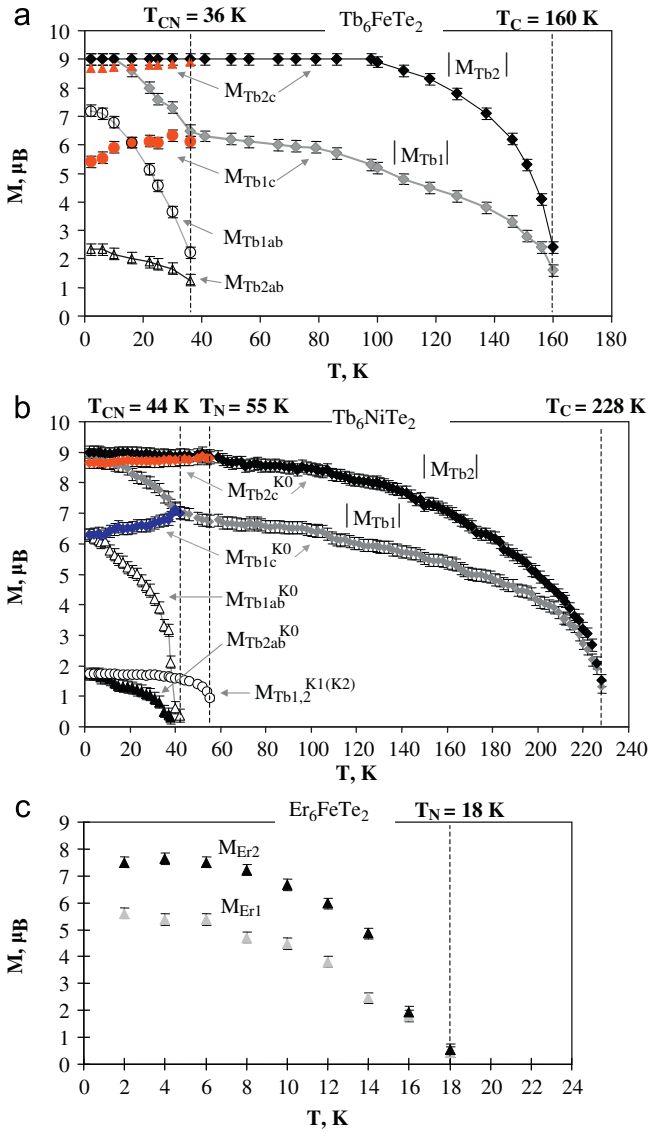

Fig. 12. Thermal variation of the magnetic moments for the *R*1 and *R*2 sites in (a) Tb_6FeTe_2, (b) Tb_6NiTe_2 and (c) Er_6FeTe_2.

nature of the transition metals : $T_C^{R6NiTe2} > T_C^{R6CoTe2} > T_C^{R6FeTe2}$ (Tables 1 and 2).

The magnetocaloric effect of Tb_6NiTe_2 ($\Delta S_{mag} = -4.86$ J/kg K at 229 K for the field change $\Delta\mu_0 H$=0–5 T) corresponds to the decrease in the symmetry of the Tb sublattice from $P\bar{6}2m$ (paramagnetic state) →**P31m** (collinear ferromagnetic ordering).

4. Conclusion

Formation of the Fe_2P-type compounds from the Mg-type rare-earth metals [6] is shown to modify the magnetic structure of the parent elements. While the magnetic ordering temperature of R_6TTe_2 is lower than those of the pure rare-earth metals, the current modification of the Mg-type lattice facilitates ferromagnetic orderings and suppresses antiferromagnetic ones. In general, the high-temperature magnetic transitions are ferromagnetic in nature and the low-temperature ones coincide with the reorientation of magnetic moments and increase in the antiferromagnetic component.

Acknowledgments

This work was supported by the Institut Laue-Langevin in experiments no. 5-31-1908.

This work was also supported by the *Russian Fund for Basic Research* through the Project no. 09-03-00173-a and by the *Indo-Russian Fund for Basic Research* through the project no. 09-03-92653-IND_a.

Thanks to O. Isnard (Institut Néel du CNRS/Université J. Fourier, BP166X, 38042 Grenoble, France), C. Ritter (Institute Laue-Langevin, 6 Rue J. Horowitz, 38042 Grenoble, France), P. Manfrinetti and A. Provino (Dipartimento di Chimica, Universita di Genova, Via Dodecaneso 31, 16146 Genova, Italy) for help in the neutron diffraction experiment and useful discussion.

This work supported by a ICDD Grant no. 05-07. The crystallographic data of Tb_6NiTe_2, Dy_6NiTe_2, Zr_6NiTe_2, Hf_6NiTe_2, Gd_6FeTe_2,

Tb_6FeTe_2, Ho_6FeTe_2, Zr_6FeTe_2 and Hf_6FeTe_2 were used with permission—© JCPDS—International Centre for Diffraction Data.

References

[1] A.V. Morozkin, J. Alloys Compd. 353 (2003) L16–L18.
[2] A.V. Morozkin, J. Alloys Compd. 358 (2003) L9–L10.
[3] A.V. Morozkin, J. Alloys Compd. 360 (2003) L1–L2.
[4] Fanqin Meng, Carmela Maliocchi, Timothy Hughbanks, J. Alloys Compd. 358 (2003) 98–103.
[5] A.V. Morozkin, V.N. Nikiforov, B. Malaman, J. Alloys Compd. 393 (2005) L6–L9.
[6] A.V. Morozkin, Yu Mozharivskyj, V. Svitlyk, R. Nirmala, O. Isnard, P. Manfrinetti, A. Provino, C. Ritter, J. Solid State Chem. 183 (2010) 1314–1325.
[7] A.V. Morozkin, J. Alloys Compd. 395 (2005) 7–16.
[8] A.V. Morozkin, O. Isnard, P. Manfrinetti, A. Provino, C. Ritter, R. Nirmala, S.K. Malik, J. Alloys Compd. 498 (2010) 13–18.
[9] Wei He, Jiliang Zhang, Lingmin Zeng, Pingli Qin, Gemei Cai, J. Alloys Compd. 443 (2007) 15–19.
[10] F. Izumi, in: R.A. Young (Ed.), The Rietveld Method, Oxford University Press, Oxford, 1993 (Chapter 13).
[11] 〈www.ill.eu, Yellow Book〉.
[12] J. Rodriguez-Carvajal, Physica B 192 (1993) 55–69.
[13] J. Emsley, The Elements, second ed., Clarendon Press, Oxford, 1991
[14] A.M. Tishin, Y.L. Spichkin, The Magnetocaloric Effect and its Applications, Institute of Physics Publishing, Bristol, Philadelphia, 2003 480 pp
[15] P.S. Kireev, Introduction of Theory Group and it's Application in Solid State Physics, High Scool, Moscow, 1979 in Russian
[16] S. Legvold, Rare earth metals and alloys, in: E.P. Wohlfarth (Ed.), Ferromagnetic Materials, North-Holland Publish. Co., Amsterdam, 1980, pp. 183–295.
[17] S.K. Malik, A.V. Morozkin, R. Nirmala, unpublished.